PAPER • OPEN ACCESS

# Indirect magnetic interaction mediated by Fermi arc and boundary reflection near Weyl semimetal surface

New Journal of Physics
The open access journal at the forefront of physics

Deutsche Physikalische Gesellschaft DPG
IOP Institute of Physics

Published in partnership with: Deutsche Physikalische Gesellschaft and the Institute of Physics

OPEN ACCESS

RECEIVED
28 May 2018

REVISED
24 August 2018

ACCEPTED FOR PUBLICATION
25 September 2018

PUBLISHED
10 October 2018



PAPER

# Indirect magnetic interaction mediated by Fermi arc and boundary reflection near Weyl semimetal surface

**Hou-Jian Duan**[1], **Shi-Han Zheng**[1], **Pei-Hao Fu**[1], **Rui-Qiang Wang**[1,3], **Jun-Feng Liu**[2,3], **Guang-Hui Wang**[1] and **Mou Yang**[1]

[1] Guangdong Provincial Key Laboratory of Quantum Engineering and Quantum Materials, School of Physics and Telecommunication Engineering, South China Normal University, Guangzhou 510006, People's Republic of China
[2] Department of Physics, Southern University of Science and Technology, Shenzhen 518055, People's Republic of China
[3] Author to whom any correspondence should be addressed.

**E-mail:** rqwanggz@163.com and liujf@sustc.edu.cn

**Keywords:** RKKY interaction, Weyl semimetal, Fermi arc

## Abstract

We theoretically investigate the Ruderman–Kittel–Kasuya–Yosida (RKKY) interaction between magnetic impurities distributed in the vicinity of the surface of a Weyl semimetal. Contrary to previous studies, we further take into account the influence of interplay of the Fermi arc and bulk states, and interface refection. It is shown that the RKKY pattern is significantly mediated by the Fermi-arc surface state along with the interface reflection. The Fermi-arc surface state mediates the RKKY interaction by interfering with the bulk states. The resulting interference contribution in the short-range impurity distance $R$ is comparable in magnitude to the bulk-band contribution and even dominates the latter near the surface. It either enhances or weakens the bulk contribution, depending on the relative orientation of impurities and Fermi energy. More importantly, for the long-range impurity distance the interference term dominates in that it can prolong the decay rate from the original bulk $R^{-5}$-law to $R^{-2}$ ($R^{-3}$) for finite (zero) Fermi energy. The interface reflection not only enhances the magnitude of the RKKY interaction and changes its anisotropy from the original XXZ to XYZ or Ising spin model, but also generates extra twisted RKKY terms parallel to the line connecting Weyl nodes, lacked in the scenario without the interface effect. They originate from the interaction between the impurity and the mirror image of the other impurity. We further analyze in detail the spatial anisotropy of the decay rate and beating pattern. These findings provide a deeper insight into surface magnetic interaction mediated by Weyl fermions.

## 1. Introduction

Advancement of novel Dirac materials is currently attracting more and more attention in condensed matter physics due to their unique band structure. Weyl semimetals (WSMs), as a newly-discovered topological state of matter, could be realized by splitting a degenerated Dirac point into two separated Weyl nodes with opposite chirality under either breaking the time-reversal or inversion symmetry [1–3]. Recently, WSMs with time-reversal symmetry have been found in the noncentrosymmetric transition-metal monosphides, including TaAs [2, 4–6], TaP [7, 8], NbP [9] and NbAs [10]. It is also expected that the WSMs with broken time-reversal symmetry also can be implemented by means of the magnetically doping technique [11–15] or applying a beam of off-resonant light [3, 16–24] . For example, the Floquet WSMs are reported if a circularly polarized light is applied to nodal line semimetals [3] or 3D Dirac semimetals [17].

Besides the linear dispersion of bulk band, the most significant feature of WSMs is the splitting nodes, which are topologically robust as long as translational symmetry is preserved and can be interpreted as a composition of a magnetic monopole and anti-monopole. They can only be created or annihilated at pair. The stable topological feature of Weyl node pairs could be characterized by the non-zero Berry curvature in the momentum space. As a consequence, the WSMs exhibit many anomaly phenomena, such as anomalous Hall effects [1, 25–29], chiral

anomaly [25, 30–32], negative magnetoresistance [33–35], and untraditional superconductivity [36, 37]. Another remarkable topological property of WSMs is the existence of topologically protected surface states. The surface states in $\mathbf{k}$-space form Fermi arc, connecting the Weyl nodes projected to the surface Brillouin zone. Different from the gapless surface state of topological insulators, which inhabits within the bulk band gap and is depart from the bulk sates, the Fermi-arc surface states in WSMs are directly connected to the bulk states. Consequently, the surface properties of WSMs are contributed by both the bulk and surface states. To detect the Fermi arc, many literatures have focused on specific impurity scattering, such as quasiparticle interference (or Friedel oscillations) [38–41] and Kondo effect [42, 43], and other interesting transport properties. However, the magnetic properties with respect to Fermi-arc states receive no attention.

Introduction of magnetic impurities to Dirac materials opens up the possibility for their application potential in spintronics. Among magnetic impurities, the effective magnetic interaction mediated by the electrons of host material, namely the Ruderman–Kittel–Kasuya–Yoshida (RKKY) interaction [44], is crucial for magnetic ordering of the impurities. The nature of the RKKY interaction is determined by the dispersion and magnetic texture in host materials, which has recently been extensively explored in Dirac materials. In graphene [45–49], it was reported that the exchange interaction between the magnetic adatoms presents isotropic decay rate with an impurity distance as $R^{-3}$, whether in the armchair direction or in the zigzag direction. Unlike graphene, phosphorene [50] exhibits strong anisotropy along different lattice directions and applied linear strain can increase the RKKY magnitude nonlinearly and prolong the decay rate from the exponent to $R^{-2}$. On the surface of three dimensional topological insulators [51, 52], it was shown that the RKKY interaction consists of the Heisenberg, Ising, and Dzyaloshinskii–Moriya (DM) terms, and the competition among them causes rich spin configurations. Very recently, several groups extended this study to the Dirac/WSMs [53–55]. For example, Chang *et al* [53] have studied the RKKY interaction in Dirac and WSMs with two impurities aligned to a specific axis, and found that the internode process as well as the spin-momentum locking has significant influence on the RKKY interaction, resulting in both a Heisenberg and an Ising term, and an additional DM term if the inversion symmetry is absent. When magnetic impurities are distributed along arbitrary orientation, Hosseini *et al* [54] reported a new spin-frustrated term, which along with the DM term lies only in the plane perpendicular to the line connecting two Weyl points but no components along the connecting line. In their studies, all RKKY terms decay fast with a spatial dependence as $R^{-5}$ for half-filling band and falls as $R^{-3}$ in finite Fermi energy. When these discussions shed new light on the WSMs, their results are suitable only for the case of magnetic impurities embedded deeply inside WSMs bulk bands, where the effect of Fermi arc and interface reflection are neglected. In reality, many interesting properties originate from the effect of surface/interface doped magnetically [56, 57].

Motivated by this, in present paper we consider magnetic impurities placed near the surface of a semi-infinite WSM and evaluate the RKKY interaction by taking into account the Fermi arc as well as the boundary reflection. It is found that the interplay between Fermi arc and bulk states near the boundary contributes the RKKY interaction with magnitude comparable with or exceeding the bulk contribution. Importantly, it can prolong the decay rate of RKKY interaction to $R^{-2}$-law, exhibiting the behavior of two-dimensional materials. With impurities close to the surface, the reflection effect significantly increase the size of RKKY interaction and generate interesting twisted RKKY terms (i.e. DM and spin-frustrated terms) parallel to the line connecting Weyl nodes, lacked in the scenario without interface effect. All the properties of RKKY interaction depend on the spatial direction of the impurity-connected line. This paper is organized as follows. In section 2, a theoretical model is provided and Green's functions for Fermi-arc surface state and reflected bulk states are derived. We analyze in detail the influence of Fermi arc along with interface reflection on the RKKY interaction in section 3. A short summary is given in the last section.

## 2. Model and method

To consider the influence of the Fermi arc on the RKKY interaction, we study a semi-infinite WSM as shown in figure 1, where a WSM is placed in the right half-plane ($y > 0$) and the vacuum in the left half-plane ($y < 0$). The surface is at $y = 0$ and infinite along $x$- and $z$- directions. Along $y$ direction, the momentum $k_y$ is not a good quantum number and replaced by an operator $k_y = -\mathrm{i}\partial_y$. For the convenience of analysis, we employ a simplest continuum model for WSMs proposed by Okugawa and Murakamii [58], which is written as

$$H = \gamma(k_z^2 - m)\sigma_z + v_f(k_x\sigma_x + k_y\sigma_y), \tag{1}$$

where $\mathbf{k} = \{k_x, k_y, k_z\}$ is the momentum, $\sigma = \{\sigma_x, \sigma_y, \sigma_z\}$ is spin Pauli operator, and $v_f$, $m$, and $\gamma$ are non-zero systemic constants. For Hamiltonian equation (1), the bulk band dispersion is $E_s = s\sqrt{v_f^2(k_x^2 + k_y^2) + \gamma^2(k_z^2 - m)^2}$, where $s = \pm$ represent conduction and valence bands. If $m$ is positive, the bulk conduction and valence bands touch each other at two Weyl points located at $(0, 0, \pm\sqrt{m})$ as shown in

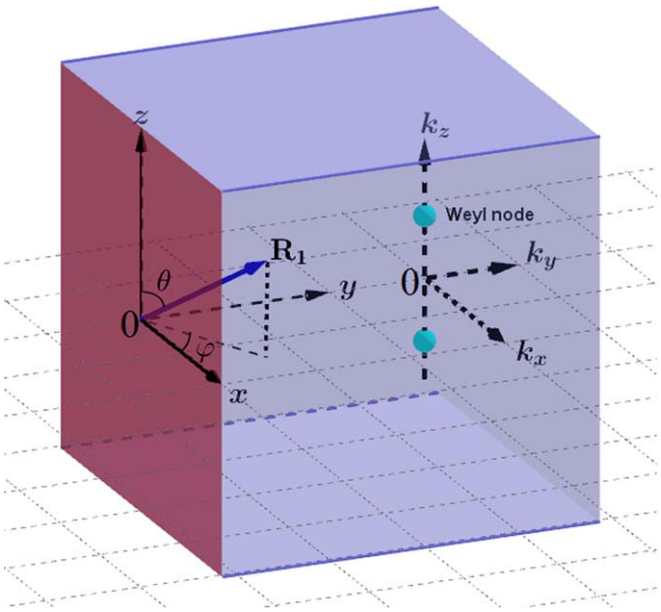


**Figure 1.** Schematic diagram for a WSM with two splitting Weyl nodes along the $k_z$ direction. The surface is at $y = 0$ and infinite along the $x$- and $z$-direction. $\mathbf{R}_1$ is the distance vector connecting the two impurities when one impurity is placed at the origin and the other in the bulk.

figure 1, describing one pair of a monopole and an anti-monopole. From this model Hamiltonian, one can calculate the surface states and bulk states on the same footing.

In order to obtain the surface state in this semi-infinite WSM, we set the magnetic term [59] $m = -\infty$ for $y < 0$ and finite in the WSM side. We assume an incident wave $Ce^{-ik_y y}$ is injected along $-y$ direction. Near the interface, if the wave is bound to the $x$–$z$ surface, the solution of wave vector $k_y$ becomes imaginary. By considering the continuity conditions of the boundary between left and right regions, one can easily obtain the surface state at $y = 0$ as

$$\Psi_{\rm sur}(k_x,\, k_z,\, \mathbf{r}) = \frac{\sqrt{\gamma'}\,\theta(y)}{2\pi} e^{i(k_x x + k_z z) - \gamma' y}\begin{pmatrix}1\\1\end{pmatrix}. \tag{2}$$

Here, $\gamma' = \gamma(m - k_z^2)/v_f$ acts as the decay factor and $\theta(y)$ denotes the Heaviside step function. The corresponding surface band reads as $E_{\rm sur} = v_f k_x$ in the range of $-\sqrt{m} < k_z < \sqrt{m}$ and vanishes otherwise. The surface state forms a Fermi arc in $\mathbf{k}$-space connecting two Weyl nodes if projected to the surface Brillouin zone.

The structure of the bulk states in the presence of the boundary differs from the case of an infinite sample in which $k_y$ is a good quantum number. Following the same processes but considering a real wave vector $k_y$, the wave function of bulk bands can be calculated as,

$$\Psi^{s\chi}_{\rm bulk}(\mathbf{k},\, \mathbf{r}) = \frac{-e^{i(k_z z + k_x x)}}{2\pi\sqrt{2\pi}}\begin{pmatrix} f^{s\chi}_{-}(\mathbf{k})\, e^{ik_y y} - \text{c.c.}\\ f^{s\chi}_{+}(\mathbf{k})\, e^{ik_y y} - \text{c.c.}\end{pmatrix}, \tag{3}$$

with

$$f^{s\chi}_{\pm}(\mathbf{k}) = \frac{s\chi v_z(k_z - \chi\sqrt{m}) \pm (sv_f k_\pm - k_\chi)}{2\sqrt{(k_\chi - sv_f k_x)k_\chi}},$$

where $v_z = 2\gamma\sqrt{m}$, $k_\chi = \sqrt{v_f^2(k_x^2 + k_y^2) + v_z^2(k_z - \chi\sqrt{m})^2}$, and $\chi = \pm 1$ denote the chirality of the two Weyl nodes. The wave function consists of two parts: an incident wave and a reflected wave. When we drop the conjugate terms in equation (3), the wave function reduces to the case without the boundary. In obtaining the analytical expression of equation (3), we have linearized the Hamiltonian (1) around the Weyl points $(0,\, 0,\, \pm\sqrt{m})$ to the low-energy model

$$H_\chi = v_f\left[(k_x\sigma_x + k_y\sigma_y) + \frac{\chi}{\lambda}(k_z - \chi\sqrt{m})\sigma_z\right], \tag{4}$$

where $\lambda = v_f/v_z$ and the energy dispersion is $E_s = sk_\chi$.

We assume that two magnetic impurities positioned at points $\mathbf{r}_A$ and $\mathbf{r}_B$ interact with WSM electrons weakly enough not to change the host dispersion. The interaction is expressed as the standard $s$-$d$ exchange Hamiltonian $H_{\rm int} = J_0\sum_{i=A,B}\mathbf{S}^i\cdot\boldsymbol{\sigma}\delta(\mathbf{r} - \mathbf{r}_i)$, where $\mathbf{S}^i$ is the local classic impurity spin. Using standard

approximating method [60–63] to the second order term of the interaction $J_0$, one at zero temperature can obtain an effective interaction between magnetic impurities,

$$H_{\mathrm{RKKY}} = -\frac{J_0^2}{\pi}\,\mathrm{Im}\int_{-\infty}^{u_F} \mathrm{d}\omega\,\mathrm{Tr}[(\mathbf{S}^A\cdot\boldsymbol{\sigma})G(\omega,\,\mathbf{r}_A,\,\mathbf{r}_B) \times(\mathbf{S}^B\cdot\boldsymbol{\sigma})G(\omega,\,\mathbf{r}_B,\,\mathbf{r}_A)], \tag{5}$$

where $G(\omega,\,\mathbf{r}_i,\,\mathbf{r}_j)$ is the retarded Green's function in frequency-real space and $u_F$ is Fermi energy. Obviously, before calculating the exchange interaction, we must first derive the retarded Green's functions. They can be constructed from the wave functions within the Lehmann's representation [64, 65]:

$$G(\omega,\,\mathbf{r}_A,\,\mathbf{r}_B) = \sum_n \frac{\Psi_n(\mathbf{r}_A)\Psi_n^{\dagger}(\mathbf{r}_B)}{\omega - E_n + \mathrm{i}\eta}, \tag{6}$$

where $\Psi_n(\mathbf{r})$ represents the $n$th eigenstate in equations (2) and (3) with the corresponding eigenenergy $E_n$. Due to the coexistence of surface and bulk wave functions, the full Green's function can be decomposed into two parts: $G(\omega,\,\mathbf{r}_A,\,\mathbf{r}_B) = G_{\mathrm{sur}}(\omega,\,\mathbf{r}_A,\,\mathbf{r}_B) + G_{\mathrm{bulk}}(\omega,\,\mathbf{r}_A,\,\mathbf{r}_B)$ with $G_{\mathrm{bulk}}(\omega,\,\mathbf{r}_A,\,\mathbf{r}_B) = \sum_{s,\chi} G_{\mathrm{bulk}}^{s\chi}(\omega,\,\mathbf{r}_A,\,\mathbf{r}_B)$, respectively, constructed by the wave functions of the surface band only or bulk states only. In this way, we can work out the analytical expressions for Green's functions. With the help of equation (2) and integrating over the momentum $\mathbf{k}$, we can obtain the Green's function contributed by the surface band,

$$G_{\mathrm{sur}}(\omega,\,\mathbf{r}_A,\,\mathbf{r}_B) = -\frac{\mathrm{i}\gamma\theta(y_A)\theta(y_B)\theta(\Delta x)\Lambda(\tilde{y},\,\Delta z)}{2\pi v_f^2}\mathrm{e}^{\mathrm{i}\omega\Delta x/v_f}\rho, \tag{7}$$

where $\rho = \sigma_x + \sigma_0$, $\tilde{y} = y_A + y_B$, and $\Lambda(\tilde{y},\,\Delta z)$ denotes an integration $\Lambda(\tilde{y},\,\Delta z) = \int_{-\sqrt{m}}^{\sqrt{m}} \mathrm{d}k_z(m - k_z^2)\mathrm{e}^{\mathrm{i}k_z\Delta z + \gamma\tilde{y}(k_z^2 - m)/v_f}$. For convenience, above and hereinafter we denote $\mathbf{R}_1 = \mathbf{r}_A - \mathbf{r}_B = (\Delta x,\,\Delta y,\,\Delta z)$, $\mathbf{R}_2 = (\Delta x,\,\tilde{y},\,\Delta z)$, and $\mathbf{R}'_{1(2)}$ denotes $\mathbf{R}_{1(2)}$ in which $\Delta z$ is replaced by $\lambda\Delta z$. Also, one can use the wave functions in equation (3) to construct the Green's function of bulk states. After integrating over the momentum, the bulk Green's function can be written analytically as

$$G_{\mathrm{bulk}}(\omega,\,\mathbf{r}_A,\,\mathbf{r}_B) = \frac{\omega\cos(\sqrt{m}\,\Delta z)}{\Omega v_f^2/(4\pi^2\lambda)}\sum_{n=1,2}\frac{\mathrm{e}^{\mathrm{i}\frac{R'_n\omega}{v_f}}}{R'_n}\left(\frac{\beta_n}{R_n'^2} - \alpha_n\right), \tag{8}$$

with

$$\beta_1 = (\mathrm{i}R'_n - v_f/\omega)[\mathrm{i}(\Delta x\sigma_x + \Delta y\sigma_y) - \lambda\Delta z\tan(\sqrt{m}\,\Delta z)\sigma_z],$$
$$\beta_2 = (\mathrm{i}R'_n - v_f/\omega)[\lambda\Delta z\tan(\sqrt{m}\,\Delta z)\sigma_z + \mathrm{i}\Delta x(2\sigma_0 + \sigma_x) + \tilde{y}\sigma_z].$$

Here, $\alpha_1 = \sigma_0, \alpha_2 = \sigma_x$, and $R'_n = |\mathbf{R}'_{\mathbf{n}}|$.

## 3. Results and discussion

Now let us turn our attention to the indirect exchange interaction between two magnetic impurities caused by the WSM electrons. Due to the presence of surface, the RKKY interaction will be mediated by the Fermi-arc surface state and the reflected bulk states. Although the Green's function can be split into the bulk and surface parts, the RKKY interactions in equation (5) cannot be simply separated to the bulk and surface components due to the interference between them. In the following, we discuss them separately. In numerical calculations, we adopt the model parameters extracted from [66]: $m = 0.0082$ Å$^{-2}$, $\gamma = 10.6424$ eV Å$^2$, $v_f = 2.4598$ eV Å.

By substituting the Green's function equation (7) or equation (2) into equation (5) and then performing careful calculations, the RKKY interaction can be written in form of

$$H_{\mathrm{RKKY}} = \sum_{i=x,y,z}[J_i S_A^i S_B^i + J_i^{\mathrm{DM}}(\mathbf{S}_A\times\mathbf{S}_B)_i] + \sum_{i=y,z} J_{xi}^{\mathrm{fr}}(S_A^x S_B^i + S_A^i S_B^x). \tag{9}$$

Here, the range function $J_i$ is the in-plane components (the Heisenberg and Ising terms), and the others are twisted component: $J_i^{\mathrm{DM}}$ for DM term, $J_{zx}^{\mathrm{fr}}$ and $J_{zy}^{\mathrm{fr}}$ for the spin-frustrated terms They are determined by the states of host electrons and the configuration of two magnetic impurities.

### 3.1. Influence of reflected bulk states on the RKKY interaction

We first consider the exchange interaction mediated by the bulk states by substituting equation (2) into (5). Due to the strong anisotropy of WSM dispersion, the RKKY interaction is also heavily dependent on the spatial orientation of distance vector between two impurities. In the following, we give both numerical and analytic results for the impurities deposited along $x$-axis and only the numerical results for other impurity configurations.

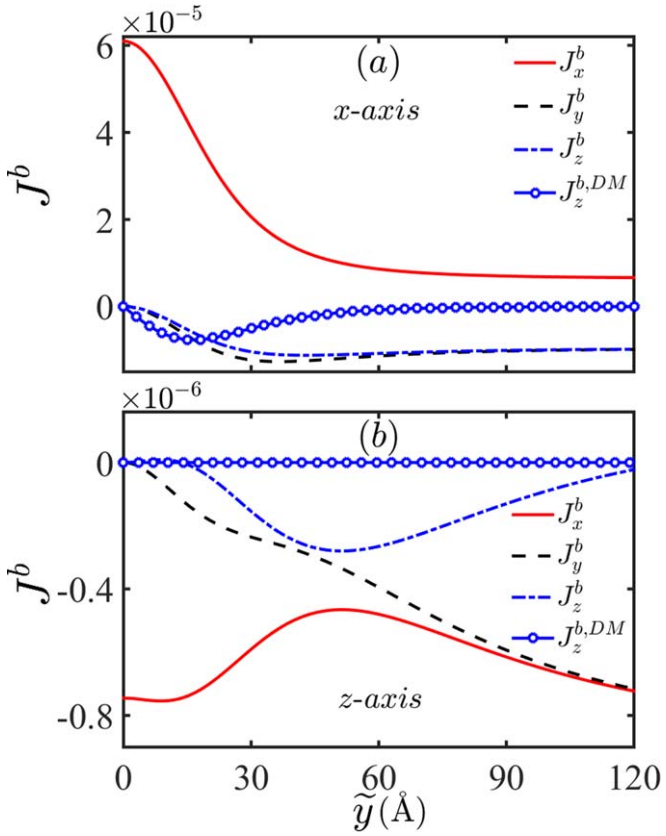


**Figure 2.** The dependence of the RKKY interaction contributed by bulk states on the spatial distance $\tilde{y}$ with respect to the boundary. Impurities are deposited (a) parallel to the $x$-axis and (b) parallel to the $z$-axis. We choose $u_F = 0$ and the relative distance of impurities $\Delta x = 40$ Å in (a) and $\Delta z = 40$ Å in (b). We take $J_0^2/\Omega^2 = 1$ as the unit of all the range functions $J$.

For impurities arranged parallel to the $x$-axis and at $u_F = 0$, the non-zero range functions read $J_z^{b,\mathrm{DM}} = -20CR_1\tilde{y}/R_2^7$,

$$J_x^b = \frac{4C}{R_1^5} - \frac{C(R_2^2 + 5\tilde{y}^2 - 25R_1^2)}{R_2^7} + I,$$
$$J_y^b = -\frac{6C}{R_1^5} + \frac{C(R_2^2 - 5\tilde{y}^2 + 15R_1^2)}{R_2^7} - I,$$
$$J_z^b = -\frac{6C}{R_1^5} + \frac{C(R_2^2 + 5\tilde{y}^2 + 15R_1^2)}{R_2^7} - I, \tag{10}$$

and the other terms vanish. Here, we denote $C = \frac{8\pi^3\lambda^2 J_0^2}{v_f\Omega^2}$ with $\Omega$ being the area of the first Brillouin zone and $I = \frac{16C(R_1^2 + R_2^2 + 3R_1R_2)}{R_1R_2^3(R_1+R_2)^3}$. In equation (10), we divide each bulk RKKY component $J_i^b$ into three parts. The first term is exactly equal to the interaction between two impurities without considering the boundary reflection. It remains unchanged no matter the distance $\tilde{y}$ of impurities away from the boundary. The second term in $J_i^b$ originates from the mirror effect, characterized by power-law decaying with the relative distance $R_2$ between the impurity A ($x_A$, $y_A$, $z_A$) and the mirror image ($x_B$, $-y_B$, $z_B$) of the impurity B with respect to the boundary. The last term in $J_i^b$ is an extra mixed term between them. Naturally, the components in the second and the third terms are significantly dependent on the impurity distance $\tilde{y}$ with respect to the boundary.

To explicitly exhibit the modification of RKKY interaction by the boundary, we in figure 2(a) display the evolutions of RKKY components for $u_F = 0$ as a function of $\tilde{y}$. In numerical calculations, we fix the relative distance between impurities (i.e., $\Delta x = \mathrm{const}$ and $\Delta z = \Delta y = 0$) and so $\tilde{y}$ denotes two times the distance of impurity pair from the boundary. Here and in the following, we take $J_0^2/\Omega^2 = 1$ as the unit of all the range functions $J$. When impurity pair is far away from the boundary ($\tilde{y}/\Delta x \gg 1$), the DM term vanishes and the impurities exhibit an XYY-like spin model ($J_x^b \neq J_y^b = J_z^b$, noticing two impurities deposited along $x$-axis). This also can be seen from equation (10), where for $\tilde{y}/\Delta x \gg 1$ or $R_2 \to \infty$, only the first term is remained in $J_i^b$. In this limit, the RKKY interaction reduces to be

$$H^{b}_{\mathrm{RKKY}} = I_1 \mathbf{S}_A \cdot \mathbf{S}_B + I_2 S^x_A S^x_B, \tag{11}$$

where $I_1 = -48\pi^3 J_0^2/(v_f \Omega^2 R_1^5)$, $I_2 = 80\pi^3 J_0^2/(v_f \Omega^2 R_1^5)$, and isotropic dispersion ($\lambda = 1$) is taken for comparison. These results recover those of bulk RKKY interaction in the absence of the boundary [53, 54]. This means that the boundary effect could be ignored if the impurity pair is located far enough away from the boundary. When the impurities move towards the boundary, all RKKY terms deviate from the above behaviors, accompanied by two significant changes. One is the quick increase of $J^b_x$ with reducing $\tilde{y}$ while overlapping $J^b_y$ and $J^b_z$ decrease in somewhat different velocity, making the spin configuration develop from original XYY to XYZ model. The anisotropy of the exchange interaction reaches the strongest at the boundary ($\tilde{y} = 0$), where only the Ising term $J^b_x$ survives while the other components are exactly compensated by the interface reflection. Another significant change is the appearance of a peculiar DM term in the vicinity of the boundary. It is noted that if the boundary is absent [54], the DM term vanishes for $u_F = 0$ and is finite only for electron–hole symmetry breaking (or $u_F \neq 0$) with its direction perpendicular to the line connecting the Weyl nodes. In contrast, in present Weyl system with boundary, the DM term emerges even for $u_F = 0$ when impurities are located in the vicinity of the boundary but not exactly at the boundary. Moreover, different from the DM term in bulk WSMs [54], here the DM term $J^{\mathrm{DM}}_z$ is parallel to the line connecting the Weyl nodes, which is contributed purely by the interaction between the impurity and the mirror image of the other impurity (indicating by $R_2$).

In figure 2(b), we depict the $\tilde{y}$-dependence of RKKY components for impurities arranged along the $z$-axis. Compared with figure 2(a), the similar change happens for this case. The main differences are: (1) the obtained RKKY interaction is almost two orders of magnitude smaller; (2) $J^b_x$ is overlapped with $J^b_y$ for large $\tilde{y}$ and in intermediate $\tilde{y}$ the spin model $XYZ$ becomes prominent. Besides, in this impurity configuration, the DM term vanishes completely. On the $x$–$z$ surface, the dependence of DM term on spatial direction can be described with $J^{b,\mathrm{DM}}_z \propto \sin(\theta_{R_1})$. Here $\theta_{R_1}$ ($\phi_{R_1}$) is the polar (azimuth) angle of $\mathbf{R}_1 = R_1(\sin\theta_{R_1}\cos\phi_{R_1}, \sin\theta_{R_1}\sin\phi_{R_1}, \cos\theta_{R_1})$ as demonstrated in figure 1, where the position of one impurity is chosen at the origin point.

We display the variation of non-zero RKKY interaction with $\tilde{y}$ with finite Fermi energy $u_F$ for impurities parallel to $x$-axis in figures 3(a), (b) and to $z$-axis in figures 3(c), (d). Also, the relative distance of two impurities is fixed as in figure 2. Remarkably, the finite Fermi energy gives rise to oscillation of all the RKKY interactions and their oscillating amplitudes decay with the distance $\tilde{y}$ measured from the boundary. The underlying physics stems from the interference between the impurity–impurity interaction and the impurity–mirror–impurity interaction, which manifests themselves as a cosine function $\cos[(R_1' + R_2')u_F/v_f]$ or $\cos(2R_2' u_F/v_f)$, where $\mathbf{R}_1' = (\Delta x, \Delta y, \lambda\Delta z)$ and $\mathbf{R}_2' = (\Delta x, \tilde{y}, \lambda\Delta z)$. At the same time, the RKKY interaction is several orders of magnitude larger than the case of $u_F = 0$ in figure 2. For impurities parallel to $x$-axis, one in figure 3(b) can notice that a new DM term $J^{\mathrm{DM}}_x$ develops for finite $u_F$, perpendicular to the line connecting Weyl nodes due to the electron–hole asymmetry. It dominates quickly over the component $J^{\mathrm{DM}}_z$. In addition, the spin-frustrated term $J^{\mathrm{fr}}_{zx}$ has non-zero components near the boundary in this case and vanishes for impurities far away from the boundary, resembling to $J^{\mathrm{DM}}_z$. $J^{\mathrm{fr}}_{zx}$ originates from the interplay of mirror effect and the electron–hole asymmetry. Figures 3(c), (d) show the case of two impurities arranged along $z$-axis, where the same RKKY oscillation emerges but without any DM term.

### 3.2. Influence of the Fermi arc on the RKKY interaction

Two impurities deposited on WSM surface interact with each other not only via the bulk states but also the surface state near the Fermi energy. In the following, we will explore the contribution of Fermi-arc surface state on RKKY components. When substituting $G_{\mathrm{sur}}(\omega, \mathbf{r}_A, \mathbf{r}_B)$ in equation (7) into equation (5), one can calculate the RKKY interaction contributed by surface state. It is easy to find that there is no overlapping between $G_{\mathrm{sur}}(\omega, \mathbf{r}_A, \mathbf{r}_B)$ and $G_{\mathrm{sur}}(\omega, \mathbf{r}_B, \mathbf{r}_A)$ for any energy $\omega$ and so purely surface state does not contribute to the exchange interaction for present two-nodal model. Physically, such zero contribution can be attributed to the open Fermi arc in single conducting channel. Similar mechanism is also addressed in [67], where the open Fermi arc at a single surface of a WSM cannot host the quantum Hall effect. Even so, the Fermi arc also mediates the RKKY interaction significantly by the interference with the bulk states, characterized by a product of bulk-state and surface-state Green's functions.

For impurities parallel to the $x$-axis, the non-zero range functions at $u_F = 0$ read

$$\begin{aligned}
J^i_x &= \frac{2\gamma C\Lambda(\tilde{y}, 0)}{v_f \lambda}\left[\frac{1}{R_1^3} - \frac{2(R_2^2 - 3R_1^2 - 6R_1R_2)}{R_2^3(R_1 + R_2)^2}\right],\\
J^i_{y,z} &= \frac{4\gamma C\Lambda(\tilde{y}, 0)}{v_f \lambda}\left[-\frac{1}{R_1^3} + \frac{1}{R_2^3}\right],\\
J^{i,\mathrm{DM}}_z &= -\frac{4\gamma C\Lambda(\tilde{y}, 0)}{v_f \lambda}\frac{(R_1 + 2R_2)\tilde{y}}{R_2^3(R_1 + R_2)^2},
\end{aligned} \tag{12}$$

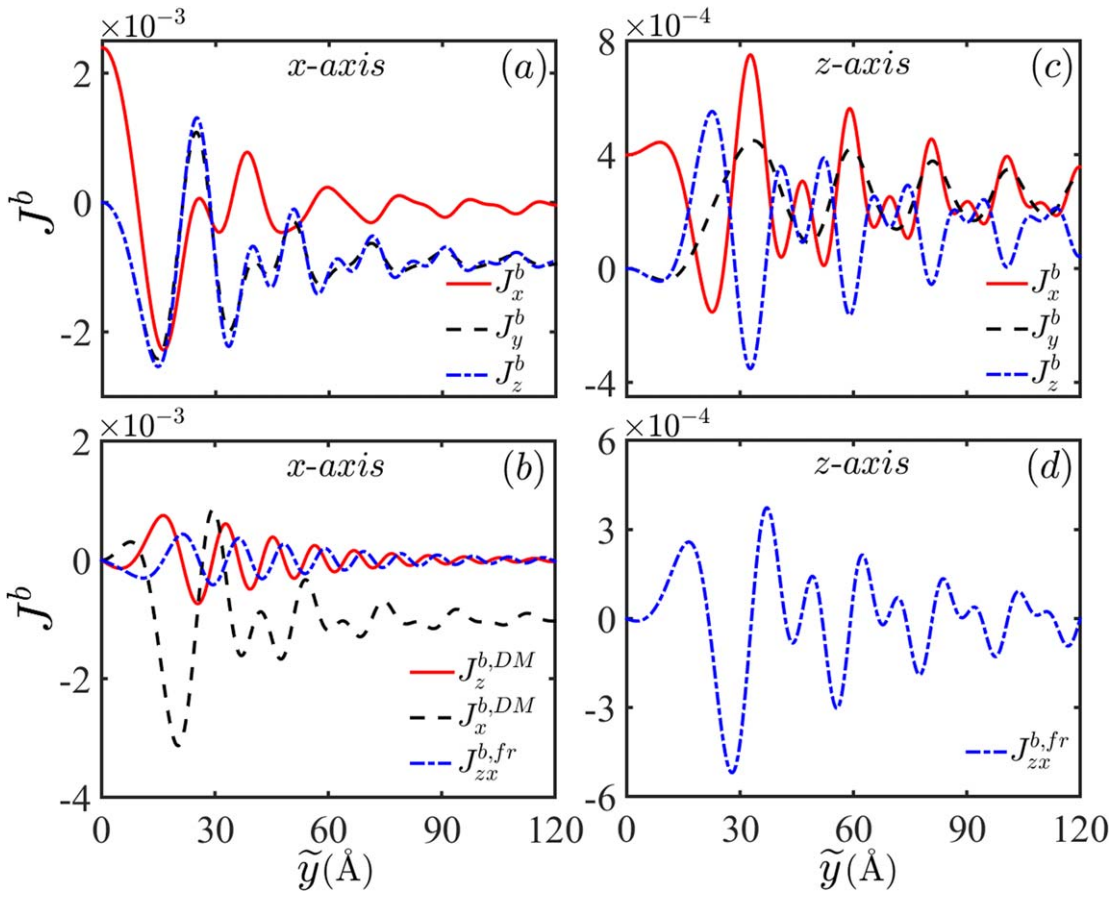


**Figure 3.** The dependence of the RKKY interaction contributed by bulk states on $\tilde{y}$ for $u_F = 4v_f\sqrt{m}$. (a), (b) Impurities are deposited parallel to the $x$-axis and (c), (d) parallel to the $z$-axis. $J_0^2/\Omega^2 = 1$ is as the unit of $J$.

and the other terms vanish. Here, all interactions depends on the integration $\Lambda(\tilde{y}, 0)$ and so $\tilde{y}$. The asymptotic behavior of $\Lambda$ is $\Lambda(\tilde{y}, 0) \approx 4m^{3/2}(v_f - m\tilde{y}\gamma)/(3v_f)$ for small $\tilde{y}$, and $\Lambda(\tilde{y}, 0) \approx \lambda v_f/(\gamma\tilde{y}^2)$ for large $\tilde{y}$.

We in figure 4(a) show the RKKY terms stemming from the interference effect as a function of spatial distance $\tilde{y}$, where two impurities are arranged parallel to the $x$-axis and $u_F = 0$. Naturally, these interference interactions vanish if impurities are far away from the boundary ($\tilde{y} \to \infty$). With the impurity pair close to the boundary, their magnitudes become visible and the spin structure behaves $XYY$-like model due to always $J_y^i = J_z^i$. More importantly, by comparing figure 4(a) with 2(a), it shows that the magnitude of the interference contribution is comparable with bulk contribution. In figures 4(b) and (c), we plot the bulk components ($J_i^b$ and $J_z^{b,\mathrm{DM}}$) and the interference components ($J_i^i$ and $J_z^{i,\mathrm{DM}}$) for comparison. Obviously, with the decrease of $\tilde{y}$, the interference components play more and more important role. For example, in figure 4(b) when the distance $\tilde{y}$ is lower than a certain position (indicated with a circle), $J_x^i$ dominates over the bulk value $J_x^b$. This specific position can be further mediated by $u_F$.

Above discussions are for two impurities resided parallel to the $x$-axis. For arbitrary impurity configurations, the competition between interference and bulk parts leads to rich behaviors. In the following, we keep at least one impurity situated at the boundary and discuss the orientation dependence of $J_x$. In figures 5(a) and (b), we plot the dependence of $J_x^b$ and $J_x^i$ on polar angle $\theta_{R_1}$ with two impurities placed at the $x$–$z$ plane (i.e. $\tilde{y} = 0$). For $u_F = 0$ in figure 5(a), the interference contribution $J_x^i$ dominates in most regimes. For impurities deposited along the $x$-axis (seeing $\theta_{R_1} = \pi/2$), both $J_x^b$ and $J_x^i$ reach the maxima. Then they oscillates with $\theta_{R_1}$ deviating from $\pi/2$. When reaching the $z$-axis (seeing $\theta_{R_1} = 0$), both components become quite small. $J_x^b$ and $J_x^i$ present either enhancing (the same sign) or compensating (opposite sign) behavior, depending on the impurity spatial direction $\theta_{R_1}$. Their relative magnitudes and signs and so the anisotropy of total RKKY interactions can be changed significantly by $u_F$, as shown in figure 5(b). For example, for $\theta_{R_1} = \pi/2$, $J_x^b$ and $J_x^i$ can be tuned to be opposite sign and compensate each other. It is noticed that there is no dependence on the azimuthal angle $\phi_{R_1}$ in previous works [53, 54] as a consequence of the azimuthal symmetry around a pair of Weyl dispersions. Here, the appearance of boundary breaks this symmetry and leads to interesting $\phi_{R_1}$-dependent RKKY interaction. In figures 5(c) and (d), we display the dependence of $J_x^b$ and $J_x^i$ on $\phi_{R_1}$, where we keep one impurity at origin point and rotate the line connecting two impurities in the $x$–$y$ plane. Remarkably, both $J_x^b$ and $J_x^i$ are sensitive to $\phi_{R_1}$ in

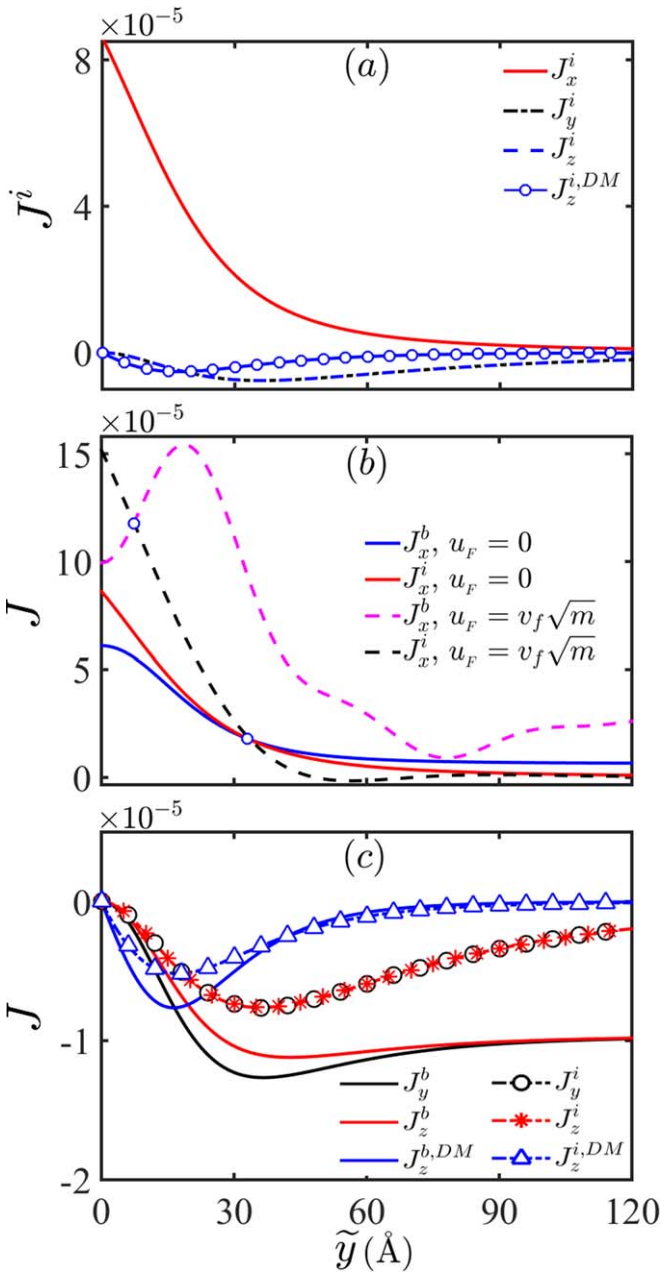


**Figure 4.** The dependence of the RKKY interaction on $\tilde{y}$ . (a) The RKKY interaction contributed purely by the interference of the Fermi arc and bulk states. (b), (c) The comparison of the bulk RKKY interactions ($J_i^b$ and $J_z^{b,\mathrm{DM}}$) and interference components ($J_i^i$ and $J_z^{i,\mathrm{DM}}$). In (b), $u_F = v_f\sqrt{m}$ is chosen and otherwise $u_F = 0$. Impurities are deposited parallel to the $x$-axis. $J_0^2/\Omega^2 = 1$ is as the unit of $J$.

magnitude and in sign. Along $x$-direction ($\phi_{R_1} = 0$), the interference term $J_x^i$ dominates over $J_x^b$ for $u_F = 0$ and compensate $J_x^b$ for finite $u_F$ due to opposite sign, as shown in figure 5(d).

Finally, we want to address the variation of bulk RKKY $J^b$ and interference RKKY interaction $J^i$ with impurity distance $R_1$. Without the boundary or for $\tilde{y} \to \infty$, the bulk RKKY interaction, namely the first term of $J_{x/y/z}^b$ in equation (10) or $I_1$ and $I_2$ in equation (11), show $R_1^{-5}$ decaying law, regardless the impurity configurations. The same results were also reported in [54]. When the boundary effect is taken into account, the second and third terms in equation (10) add two fast decaying rates, which are dependent on the distance $\tilde{y}$ with respect to the boundary. They decay as $R_1^{-6}$ or $R_1^{-7}$ for large $\tilde{y}$ and vanish at the surface. Thus, the decay rate of RKKY interactions still dominates by $R_1^{-5}$-law. Remarkably different from this, we find that the interference terms $J_{x/y/z}^i$ between Fermi arc and bulk states significantly change this scenario. To shed light on this, we derive an analytical expression for impurities situated at the interface along $x$-axis with $R_1 \gg 1$,

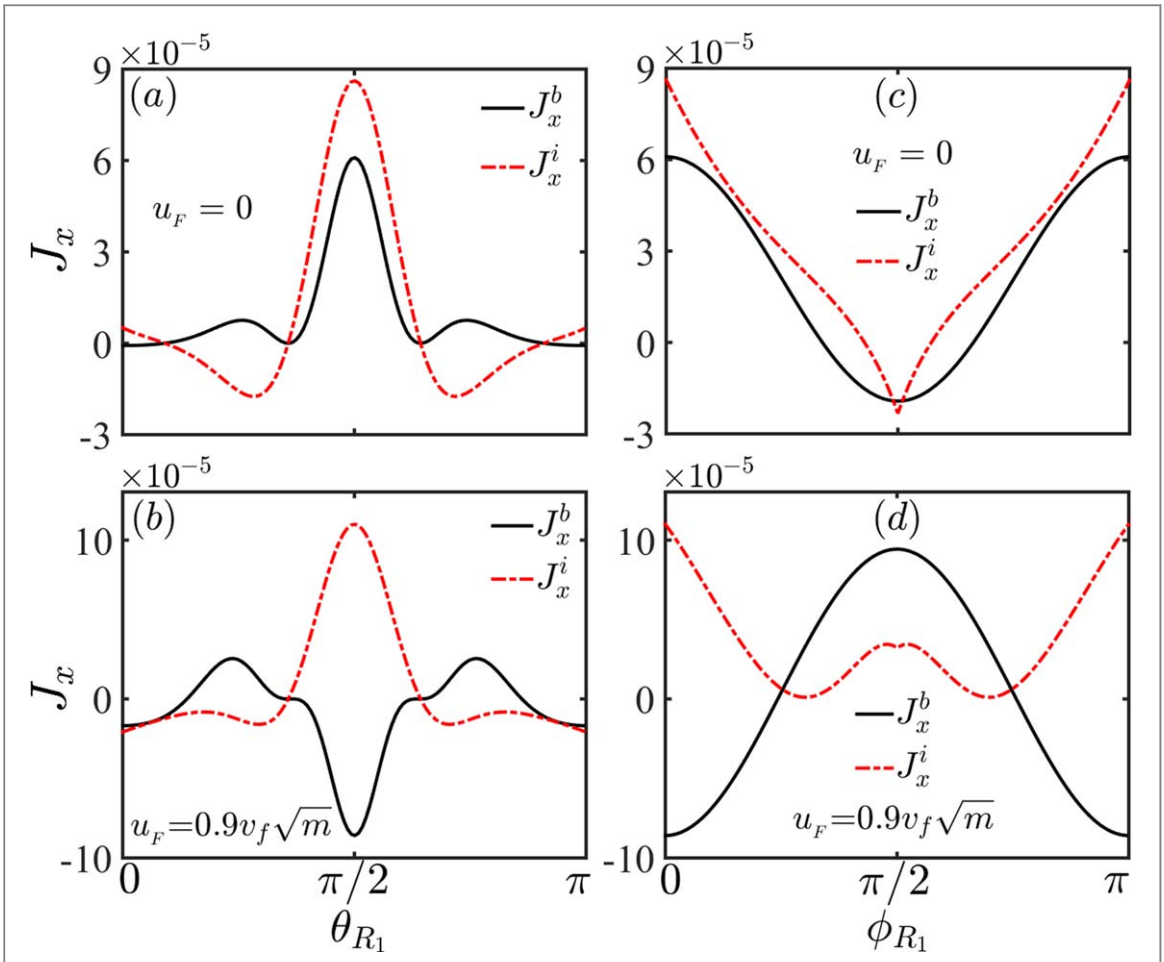


**Figure 5.** Dependence of the orientation of $J_x^b$ and $J_x^i$. We keep one impurity at the origin point and rotate (a), (b) the polar angle $\theta_{R_1}$ of $\mathbf{R}_1$ in $x$–$z$ plane, and (c), (d) the azimuthal angle $\phi_{R_1}$ in $x$–$y$ plane. The upper panels (a), (c) for $u_F = 0$ and the lower panels (b), (d) for $u_F = 0.9 v_f \sqrt{m}$. The distance between two impurities is fixed $R_1 = 40$ Å. $J_0^2/\Omega^2 = 1$ is as the unit of $J$.

$$J_x^i \approx \frac{4mC}{3\lambda^2}\left[\frac{5\cos(2u_F R_1/v_f)}{R_1^3} + \frac{2u_F \sin(2u_F R_1/v_f)}{v_f R_1^2}\right]. \tag{13}$$

Intriguingly, the interference component causes quite slowly decaying rate compared with bulk component $J_x^b$. The decay rate with impurity relative distance $R_1$ depends on the Fermi energy $u_F$, which is $R_1^{-3}$-law for $u_F = 0$ and $R_1^{-2}$-law for finite $u_F$. In this case, the interference component plays a crucial role and therefore dominates over the bulk contribution for large $R_1$. This long range behave resembles to the case in two-dimensional metal material [68]. For impurities situated at the interface but along $z$-axis (parallel to the line connecting the two Weyl points), we find

$$J_x^i \approx \frac{16C\cos^2(\sqrt{m}R_1)}{\lambda^4\sqrt{m}}[\sqrt{m}R_1 - \tan(\sqrt{m}R_1)] \times\left[\frac{\cos(\lambda R_1 u_F/v_f)}{\lambda R_1^6} + \frac{u_F \sin(\lambda R_1 u_F/v_f)}{v_f R_1^5}\right], \tag{14}$$

which instead shows $R^{-5}$-decaying rate for $u_F = 0$ and $R^{-4}$-decaying rate for finite $u_F$. Obviously, the RKKY along $z$-direction decays faster than along $x$-direction, exhibiting the significant anisotropy of the RKKY interaction.

Interestingly, for two impurities placed along $z$-axis, from equation (14) one can see that there are two periodic functions: one is $2\mathrm{T}_1$ ($T_1 = \pi v_f/(\lambda u_F)$) coming from the finite Fermi energy and the other is $T_2 = \pi/\sqrt{m}$ coming from the separated Weyl nodes. By setting appropriate $u_F$, we can observe a beating pattern either for interference component $J_x^i$ or for bulk component [54] $J_x^b$, as demonstrated in figure 6(a). Careful comparison shows that the fast oscillator period of $J_x^i$ is just two times one of $J_x^b$. In order to understand it, we derive the oscillation part $J_x^b \propto \cos^2(\sqrt{m_1}\Delta z)\cos(2u_F R_1'/v_f)$ and $J_x^i \propto \cos^2(\sqrt{m_1}\Delta z)\cos[u_F(\Delta x + R_1')/v_f]$ with $R_1' = \sqrt{(\Delta x)^2 + \lambda^2(\Delta z)^2}$. For impurities situated at the surface along $z$-axis where $\Delta x = 0$, the fast oscillator period of $J_x^i$ is naturally two times one of $J_x^b$. For arbitrary direction of impurity arrangement, their

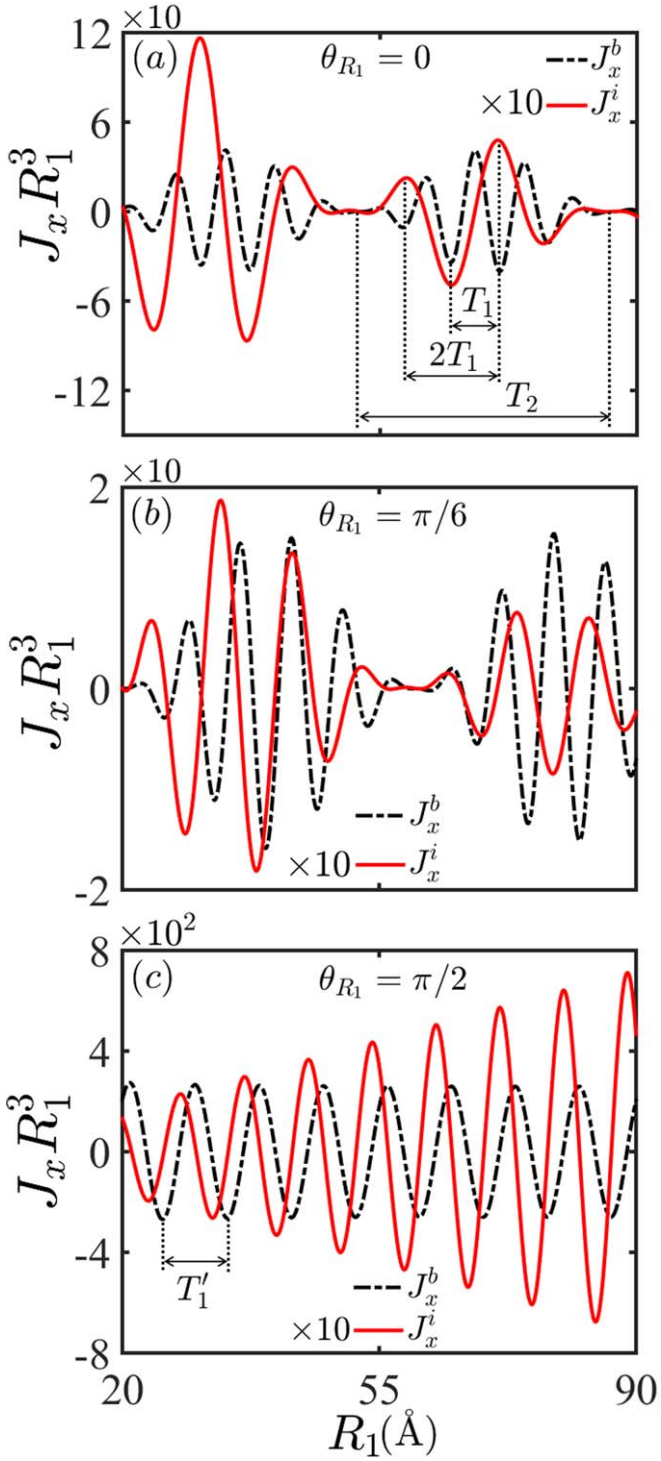


**Figure 6.** The dependence of $J_x R_1^3$ on $\theta_{R_1}$ with impurities deposited at the $x$–$z$ surface for $u_F = 4v_f\sqrt{m}$. (a), (c) Two impurities are arranged along $\theta_{R_1} = 0$ (or $z$-axis), $\theta_{R_1} = \pi/6$, and $\theta_{R_1} = \pi/2$ (or $x$-axis), respectively. In (a), $T_1 = \pi v_f/(\lambda u_F)$ and $T_2 = \pi/\sqrt{m}$. $J_0^2/\Omega^2 = 1$ is as the unit of $J$.

periods present the dependence on impurity relative direction $\theta_{R_1}$, as shown in figure 6(b). When impurities are along $x$-axis ($\theta_{R_1} = \pi/2$), the oscillation of $T_2$ vanishes and so do the beating frequency. This reveals that the beating pattern of indirect exchange interaction is anisotropic and depends tightly on the direction of impurities. The underlying mechanism stems from the spin-momentum entanglement.

## 4. Summary

We have explored the RKKY interaction between magnetic impurities mediated by Weyl fermions. Contrary to all previous studies [53–55], we further take into account the influence of interplay of Fermi arc and bulk states and interface refection. In the presence of the boundary, the bulk states and its interference with Fermi arc acquire non-trivial structure, that complicates the form of the indirect exchange interaction. It is found that there emerge rich magnetic interactions, including Heisenberg, Ising, DM, and spin-frustrated terms We first consider the contribution from boundary reflection. With impurities close to the boundary, the reflection effect becomes more and more important, on one hand, significantly increasing the size of RKKY interaction and on the other hand changing the anisotropy from the original XXZ to XYZ spin model and finally to Ising one. The boundary reflection also generate interesting DM term near the boundary. This is the consequence of the absence of the translational invariance perpendicular to the boundary. Then, we analyze the contribution from Fermi-arc surface state, which mainly interferes with bulk states and modifies the RKKY interaction with magnitude comparable with or exceeding the bulk contribution. It either enhances or weakens the bulk contribution, depending on the relative orientation of two impurities and Fermi energy. More importantly, for some specific configuration of magnetic impurities, the interference term can fall off as $R^{-3}$ for zero Fermi energy or $R^{-2}$ for finite Fermi energy, much more slowly than $R^{-5}$ in the bulk contribution, displaying a typical behavior in a two-dimensional metal. The direction dependence of the RKKY beating pattern are discussed. It is expected that these RKKY interactions can be probed experimentally by broadband electron spin resonance technique coupled with an optical detection scheme [69].

## Acknowledgments

This work was supported by GDUPS (2017), by National Natural Science Foundation of China (Grant Nos. 11474106, 11774144, 11874016, and 11274124) and by the Key Program for Guangdong NSF of China (Grant No. 2017B030311003), and the Science and Technology Program of Guangzhou City of China (Grant No. 201707010403).

## ORCID iDs

Rui-Qiang Wang https://orcid.org/0000-0002-7112-3230
Mou Yang https://orcid.org/0000-0002-3716-0652

## References

[1] Burkov A A and Balents L 2011 *Phys. Rev. Lett.* **107** 127205
[2] Xu S-Y *et al* 2015 *Science* **349** 613
[3] Hübener H, Sentef M A, Giovannini U D, Kemper A F and Rubio A 2017 *Nat. Commun.* **8** 13940
[4] Lv B Q *et al* 2015 *Phys. Rev.* X **5** 031013
[5] Weng H, Fang C, Fang Z, Bernevig B A and Dai X 2015 *Phys. Rev.* X **5** 011029
[6] Huang S-M *et al* 2015 *Nat. Commun.* **6** 7373
[7] Xu N *et al* 2016 *Nat. Commun.* **7** 11006
[8] Xu S-Y *et al* 2015 *Sci. Adv.* **1** e1501092
[9] Shekhar C *et al* 2015 *Nat. Phys.* **11** 645
[10] Xu S-Y *et al* 2015 *Nat. Phys.* **11** 748
[11] Cho G Y 2012 arXiv:1110.1939
[12] Chang C-Z *et al* 2013 *Science* **340** 167
[13] Kou X *et al* 2014 *Phys. Rev. Lett.* **113** 137201
[14] Checkelsky J G, Yoshimi R, Tsukazaki A, Takahashi K S, Kozuka Y, Falson J, Kawasaki M and Tokura Y 2014 *Nat. Phys* **10** 731
[15] Chang C-Z, Zhao W, Kim D Y, Zhang H, Assaf B A, Heiman D, Zhang S-C, Liu C, Chan M H W and Moodera J S 2015 *Nat. Mater.* **14** 473
[16] Yan Z and Wang Z 2016 *Phys. Rev. Lett.* **117** 087402
[17] Wang R, Wang B, Shen R, Sheng L and Xing D Y 2014 *Europhys. Lett.* **105** 17004
[18] Zou J-Y and Liu B-G 2016 *Phys. Rev.* B **93** 205435
[19] Chan C-K, Oh Y-T, Han J H and Lee P A 2016 *Phys. Rev.* B **94** 121106(R)
[20] Wang H, Zhou L and Chong Y D 2016 *Phys. Rev.* B **93** 144114
[21] Narayan A 2016 *Phys. Rev.* B **94** 041409(R)
[22] Taguchi K, Xu D-H, Yamakage A and Law K T 2016 *Phys. Rev.* B **94** 155206
[23] Kitagawa T, Berg E, Rudner M and Demler E 2010 *Phys. Rev.* B **82** 235114
[24] Fu P-H, Duan H-J, Wang R-Q and Chen H 2017 *Phys. Lett.* A **381** 3499
[25] Yang K-Y, Lu Y-M and Ran Y 2011 *Phys. Rev.* B **84** 075129
[26] Wan X, Turner A M, Vishwanath A and Savrasov S Y 2011 *Phys. Rev.* B **83** 205101
[27] Xu G, Weng H, Wang Z, Dai X and Fang Z 2011 *Phys. Rev. Lett.* **107** 186806

[28] Jiang Q-D, Jiang H, Liu H, Sun Q-F and Xie X C 2015 *Phys. Rev. Lett.* **115** 156602
[29] Yang S A, Pan H and Zhang F 2015 *Phys. Rev. Lett.* **115** 156603
[30] Nielsen H B and Ninomiya M 1983 *Phys. Lett.* B **130** 389
[31] Vazifeh M M and Franz M 2013 *Phys. Rev. Lett.* **111** 027201
[32] Parameswaran S A, Grover T, Abanin D A, Pesin D A and Vishwanath A 2014 *Phys. Rev.* X **4** 031035
[33] Son D T and Spivak B Z 2013 *Phys. Rev.* B **88** 104412
[34] Burkov A A 2014 *Phys. Rev. Lett.* **113** 247203
[35] Lu H-Z, Zhang S-B and Shen S-Q 2015 *Phys. Rev.* B **92** 045203
[36] Cho G Y, Bardarson J H, Lu Y-M and Moore J E 2012 *Phys. Rev.* B **86** 214514
[37] Lu B, Yada K, Sato M and Tanaka Y 2015 *Phys. Rev. Lett.* **114** 096804
[38] Zheng H *et al* 2016 *ACS Nano* **10** 1378
[39] Inoue H, Gyenis A, Wang Z, Li J, Oh S W, Jiang S, Ni N, Bernevig B A and Yazdani A 2016 *Science* **351** 1184
[40] Batabyal R, Morali N, Avraham N, Sun Y, Schmidt M, Felser C, Stern A, Yan B and Beidenkopf H 2016 *Sci. Adv.* **2** e1600709
[41] Hosur P 2012 *Phys. Rev.* B **86** 195102
[42] Principi A, Vignale G and Rossi E 2015 *Phys. Rev.* B **92** 041107(R)
[43] Mitchell A K and Fritz L 2015 *Phys. Rev.* B **92** 121109(R)
[44] Bloembergen N and Rowland T J 1955 *Phys. Rev.* **97** 1679
[45] Saremi S 2007 *Phys. Rev.* B **76** 184430
[46] Black-Schaffer A M 2010 *Phys. Rev.* B **81** 205416
[47] Sherafati M and Satpathy S 2011 *Phys. Rev.* B **83** 165425
[48] Kogan E 2011 *Phys. Rev.* B **84** 115119
[49] Lee H, Mucciolo E R, Bouzerar G and Kettemann S 2012 *Phys. Rev.* B **86** 205427
[50] Duan H-J, Li S, Zheng S-H, Sun Z, Yang M and Wang R-Q 2017 *New J. Phys.* **19** 103010
[51] Abanin D A and Pesin D A 2011 *Phys. Rev. Lett.* **106** 136802
[52] Zhu J-J, Yao D-X, Zhang S-C and Chang K 2011 *Phys. Rev. Lett.* **106** 097201
[53] Chang H-R, Zhou J, Wang S-X, Shan W-Y and Xiao D 2015 *Phys. Rev.* B **92** 241103(R)
[54] Hosseini M V and Askari M 2015 *Phys. Rev.* B **92** 224435
[55] Mastrogiuseppe D, Sandler N and Ulloa S E 2016 *Phys. Rev.* B **93** 094433
[56] Honolka J *et al* 2012 *Phys. Rev. Lett.* **108** 256811
[57] Wray L A, Xu S-Y, Xia Y, Hsieh D, Fedorov A V, Hor Y S, Cava R J, Bansil A, Lin H and Hasan M Z 2011 *Nat. Phys.* **7** 32
[58] Okugawa R and Murakami S 2014 *Phys. Rev.* B **89** 235315
[59] Gorbar E V, Miransky V A, Shovkovy I A and Sukhachov P O 2016 *Phys. Rev.* B **93** 235127
[60] Ruderman M A and Kittel C 1954 *Phys. Rev.* **96** 99
[61] Kasuya T 1956 *Prog. Theor. Phys.* **16** 45
[62] Yosida K 1957 *Phys. Rev.* **106** 893
[63] Mattis D C 2006 *The Theory of Magnetism Made Simple: An Introduction to Physical Concepts and to Some Useful Mathematical Methods* (Singapore: World Scientific)
[64] Kurilovich V D, Kurilovich P D and Burmistrov I S 2017 *Phys. Rev.* B **95** 115430
[65] Zare M, Parhizgar F and Asgari R 2016 *Phys. Rev.* B **94** 045443
[66] Wang Z, Sun Y, Chen X-Q, Franchini C, Xu G, Weng H, Dai X and Fang Z 2012 *Phys. Rev.* B **85** 195320
[67] Wang C M, Sun H-P, Lu H-Z and Xie X C 2017 *Phys. Rev. Lett.* **119** 136806
[68] Fischer B and Klein M W 1975 *Phys. Rev.* B **11** 2025
[69] Laplane C, Cruzeiro E Z, Fröwis F, Goldner P and Afzelius M 2016 *Phys. Rev. Lett.* **117** 037203